Seong et al. Huntingtin stimulates polycomb repressive complex 2

Supporting Information

Supporting Information Tables

S Table 1. Most frequent peptides (top 20%) from the Htt150 kDa tryptic fragment

S Table 2. Most frequent peptides (top 20%) from the Htt200 kDa tryptic fragment

Supporting Information Figure Legends

S Figure 1
S Figure 2
S Figure 3
S Figure 4

Supporting Information Figures

S Figure 1
S Figure 2
S Figure 3
S Figure 4

S Table 1. Most frequent peptides (top 20%) from the Htt150 kDa tryptic fragment

Huntingtin Location (Residues)	Amino Acid Sequence
119-125	NSPEFQK
126-146	LLGIAMELFLLCSDDAESDVR
147-155	MVADECLNK
159-167	ALMDSNLPR
168-174	LQLELYK
192-203	FAELAHLVRPQK
221-236	RPEESVQETLAAAVPK
237-251	IMASFGNFANDNEIK
256-262	AFIANLK
322-332	YLVPLLQQQVK
388-410	TPPPELLQTLTAVGGIGQLTAAK
445-460	VLLGEEEALEDDSESR
461-473	SDVSSSALTASVK
461-502	SDVSSSALTASVKDEISGELAASSGVSTPGSAGHDIITEQPR
474-502	DEISGELAASSGVSTPGSAGHDIITEQPR
621-633	NSSMALQQAHLLK
668-688	IKGDIGQSTDDDSAPLVHCVR
670-688	GDIGQSTDDDSAPLVHCVR
689-700	LLSASFLLTGGK
715-735	ALALSCVGAAVALHPESFFSK
739-767	VPLDTTEYPEEQYVSDILNYIDHGDPQVR
798-814	TLTGNTFSLADCIPLLR
827-833	LACTAVR
860-867	NSSYWLVR
868-880	TELLETLAEIDFR
881-888	LVSFLEAK
909-924	VLNNVVIHLLGDEDPR
927-935	HVAAASLIR
944-957	CDQGQADPVVAVAR
958-965	DQSSVYLK
966-984	LLMHETQPPSHFSVSTITR
988-1006	GYNLLPSITDVTMENNLSR
1007-1021	VIAAVSHELITSTTR
1150-1168	VINICAHVLDDVAPGPAIK
1169-1184	AALPSLTNPPSLSPIR

S Table 2. Most frequent peptides (top 20%) from the Htt200 kDa tryptic fragment

Huntingtin Location (Residues)	Amino acid sequence
1254-1264	VTLDLQNSTEK
1306-1319	EPMMATVCVQQLLK
1320-1339	TLFGTNLASQFDGLSSNPSK
1379-1398	NMVQAEQENDTSGWFDVLQK
1405-1412	TNLTSVTK
1418-1425	NAIHNHIR
1426-1433	LFEPLVIK
1449-1461	QVLDLLAQLVQLR
1480-1490	QFEYIEVGQFR
1522-1534	IIQLCDGIMASGR
1536-1555	AVTHAIPALQPIVHDLFVLR
1571-1579	EVVVSMLLR
1580-1599	LIQYHQVLEMFILVLQQCHK
1611-1622	QIADIILPMLAK
1684-1697	VLISQSTEDIVLSR
1716-1732	LRDGDSTSTLEEHSEGK
1736-1744	NLPEETFSR
1870-1887	LLSPQMSGEEEDSDLAAK
1948-1962	NSAASGLFIQAIQSR
1963-1973	CENLSTPTMLK
1975-1997	TLQCLEGIHLSQSGAVLTLYVDR
2009-2016	MVDILACR
2017-2040	RVEMLLAANLQSSMAQLPMEELNR
2018-2040	VEMLLAANLQSSMAQLPMEELNR
2041-2053	IQEYLQSSGLAQR
2057-2063	LYSLLDR
2066-2099	LSTMQDSLSPSPPVSSHPLDGDGHVSLETVSPDK
2114-2127	SDSALLEGAELVNR
2164-2171	SALFEAAR
2178-2206	VSGTVQQLPAVHHVFQPELPAEPAAYWSK
2207-2225	LNDLFGDAALYQSLPTLAR
2226-2236	ALAQYLVVVSK
2340-2356	AISEEEEEVDPNTQNPK
2357-2381	YITAACEMVAEMVESLQSVLALGHK
2383-2395	NSGVPAFLTPLLR
2396-2403	NIIISLAR
2404-2412	LPLVNSYTR
2455-2463	INTLGWTSR
2554-2566	GIVEQEIQAMVSK
2568-2598	ENIATHHLYQAWDPVPSLSPATTGALISHEK

2599-2607	LLLQINPER
2608-2615	ELGSMSYK
2684-2692	WILPSSSAR
2694-2704	TPAILISEVVR
2705-2716	SLLVVSDLFTER
2717-2730	NQFELMYVTLTELR
2732-2750	VHPSEDEILAQYLVPATCK
2751-2759	AAAVLGMDK
2760-2767	AVAEPVSR
2768-2774	LLESTLR
2782-2802	VGALHGVLYVLECDLLDDTAK
2803-2817	QLIPVISDYLLSNLK
2887-2895	LLLSEQLSR
2896-2903	LDAESLVK
2940-2959	TSDPNPAAPDSESVIVAMER
2960-2966	VSVLFDR
2981-2998	ILPQFLDDFFPPQDIMNK
2999-3020	VIGEFLSNQQPYPQFMATVVYK
3021-3035	VFQTLHSTGQSSMVR
3103-3111	HQIEEELDR
3103-3112	HQIEEELDRR
3113-3130	AFQSVLEVVAAPGSPYHR

Supporting Information Figure legends

S Figure 1 – Purification of recombinant FLAG-huntingtins

Panel A Plot (top) of Superose 6^{TM}10/300 gel filtration column elution profile of FLAG-bead enriched protein. Coomassie blue stained bands on SDS PAGE (bottom left), demonstrate a discrete peak of Q23 huntingtin (Htt) well separated from the void volume protein peak (*). The column profiles were similar for Q32 and Q43 huntingtins (data not shown). Calibration standards: High MW marker (B: Blue Dextran, T: Thyroglobulin (670 kDa), F: Ferritin (440 kDa), C: Catalase (232 kDa), A: Aldolase (150 kDa). SDS PAGE (bottom right) intact highly purified >350 kDa Q23 huntingtin in pooled peak fractions (13.0 – 14.0 ml) by Coomassie Blue stain (lane 1) and immunoblot analysis with amino terminal mAb 2166 (lane 2) and HF1 carboxyl terminal huntingtin antibody (lane 3). Similar purification data for full-length Q32- and Q43 huntingtin is not shown.

Panel B SDS PAGE Coomassie blue stain and immunoblot analysis of recombinant FLAG Q23, Q32, Q43-huntingtins reveals the impact of increasing the polyglutamine region in disproportionally decreasing huntingtin mobility and increasing mAb 1F8 detectability of the polyglutamine tract, as reported for endogenous huntingtins (10, 58, 59). Marker (M).

S Figure 2 – Negative stain EM analysis of Q23, Q32 and Q43 huntingtins

Panel A The 100 class averages resulting from classification of 10,000 interactively selected particles of negatively stained Q23 huntingtin. While the class averages show distinct structural features, these vary greatly between different classes. Since SDS PAGE and mass spectrometry analysis revealed high purity, the majority of classes should represent huntingtin. Adsorption to the carbon support film in different orientations is unlikely to account for all of the structural variability, indicating that huntingtin is a flexible molecule that can adopt different conformations, The side length of the individual class averages is 28.8 nm, demonstrating the varied structure variability.

Panel B Raw image (left) and 100 class averages resulting from classification of 10,061 particle images of negatively stained Q32 huntingtin. Bottom: Raw image (left) and 100 class averages resulting from classification of 10,078 particle images of negatively stained Q43 huntingtin, showing that the structural variability of huntingtins with different polyglutamine regions is similar to that of Q23 huntingtin. The scale bars represent 50 nm and the side length of the panels showing individual class averages is 28.8 nm.

S Figure 3 – Normal histone H3K27 di-methylation and nuclear huntingtin PRC2

Panel A Fluorescent microscope images of immunostained embryoid body sections show decreased histone H3K27me3 signal in $Hdh^{ex/4/5}/Hdh^{ex/4/5}$ cells, at day 4 and day 6, but levels similar to wild-type Hdh^{+}/Hdh^{+} cells at day 11, indicating inefficient histone H3K27 tri-methylation in the absence of huntingtin.

Panel B Confocal images of immunostained sections of day 4 Hdh^{+}/Hdh^{+} (WT) and $Hdh^{ex/4/5}/Hdh^{ex/4/5}$ (KO) huntingtin null and knock-in Hdh^{+}/Hdh^{Q111} (KI) embryoid bodies, revealed similar histone H3K27me2 stain and plot of immunoblot histone H3K27me2/H3 band intensity ratio, normalized to wild-type (white bar), confirmed similar levels of histone H3K27me2 in KO (black bar) and KI (grey bar), compared to wild-type (white bar) extracts (n=4).

Panel C Immunoblot demonstrating huntingtin (~ 350 kDa), detected by mAb 2166, in wild-type Hdh^{+}/Hdh^{+} ES cell total extract (T), as well as the cytosolic (C) and nuclear (N) sub-cellular fractions. Bands of tubulin and fibrillarin indicate purity of the cysolic and nuclear extracts, respectively.

Panel D Immunoblot (left) showing huntingtin, from day 4 wild-type Hdh^{+}/Hdh^{+} embryoid body nuclei, detected in Superose 6^{TM} HR 16/60 size exclusion chromatography fractions, together with Ezh2 and Suz12, eluting with a peak size of ~810 kDa. Size standards (arrowheads): Thyroglobulin (670 kDa), Ferritin (440 kDa), Catalase (232 kDa). Huntingtin and Ezh2 in peak fractions co-immunoprecipitated (data not shown).

S Figure 4 – Huntingtin stimulated PRC2 tri-methylation *in vitro*

Panel A Autoradiogram (top) of bands of ^{3}H-methyl histone H3 produced by reconstituted PRC2, and plot (below) of quantified band intensities (3 experiments), relative to no added huntingtin (0 Htt), demonstrating that Q23 huntingtin (Htt) significantly (*P < 0.05) stimulated PRC2 activity in a dose (2-40 nM) dependent manner.

Panel B Autoradiogram (top) showing ^{3}H-methyl histone H3 bands, and plot (bottom) of the quantified band intensities (no huntingtin open bar, added huntingtin filled bar) (3 experiments), demonstrating that Q23 huntingtin (Htt) significantly (*P< 0.05) stimulated PRC2 over a range of nucleosome array concentrations (25 – 100 nM).

Panel C Immunoblot (top) showing bands of di-methyl (H3K27me2) and tri-methyl (H3K27me3) histone H3, and plot (below) of quantified ratio of the H3K27me2/H3 and H3K27me3/H3 histone band intensities from 3 experiments, normalized to ratios obtained in the absence (white bar) or presence of huntingtin (Htt) (black bar), demonstrating that the presence (+) of Q23 huntingtin (Htt) significantly (*P < 0.05) increased PRC2-dependent tri-methyl histone H3K27, but decreased di-methyl histone H3K27, compared to reactions without added huntingtin (-).

S Figure 1

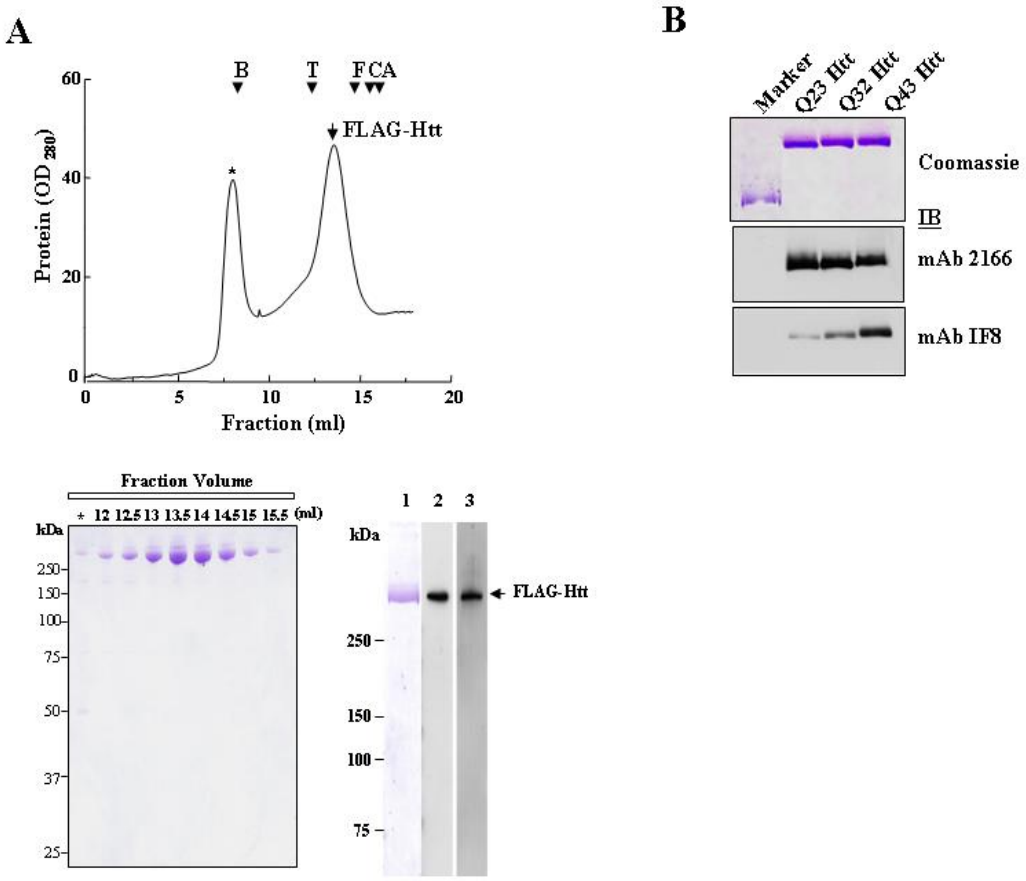
A
B
T
FCA
FLAG-Htt
Protein (OD 280)
Fraction (ml)
Fraction Volume
kDa
(ml)
FLAG-Htt
B
Marker
Q23 Htt
Q32 Htt
Q43 Htt
Coomassie
IB
mAb 2166
mAb IF8

S Figure 2

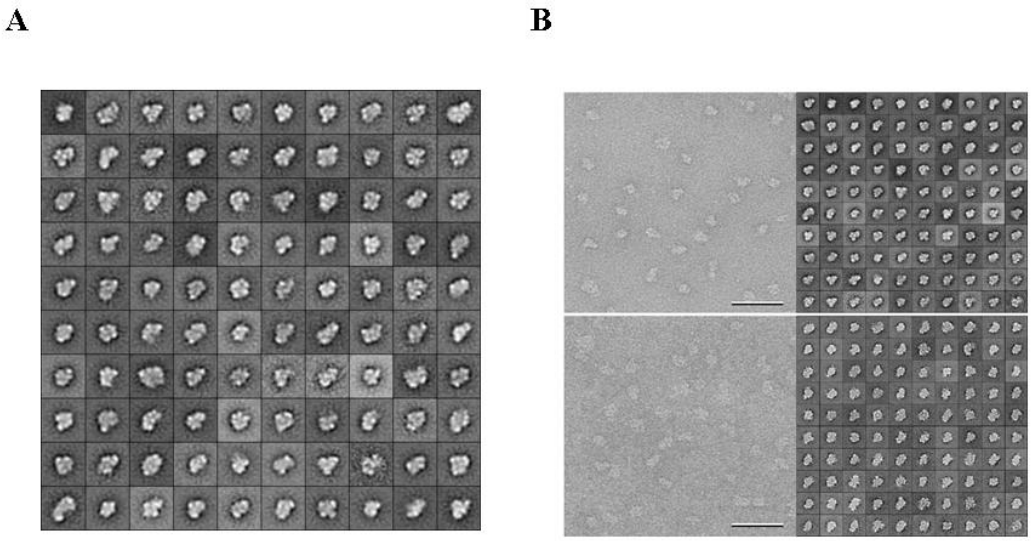

S Figure 3

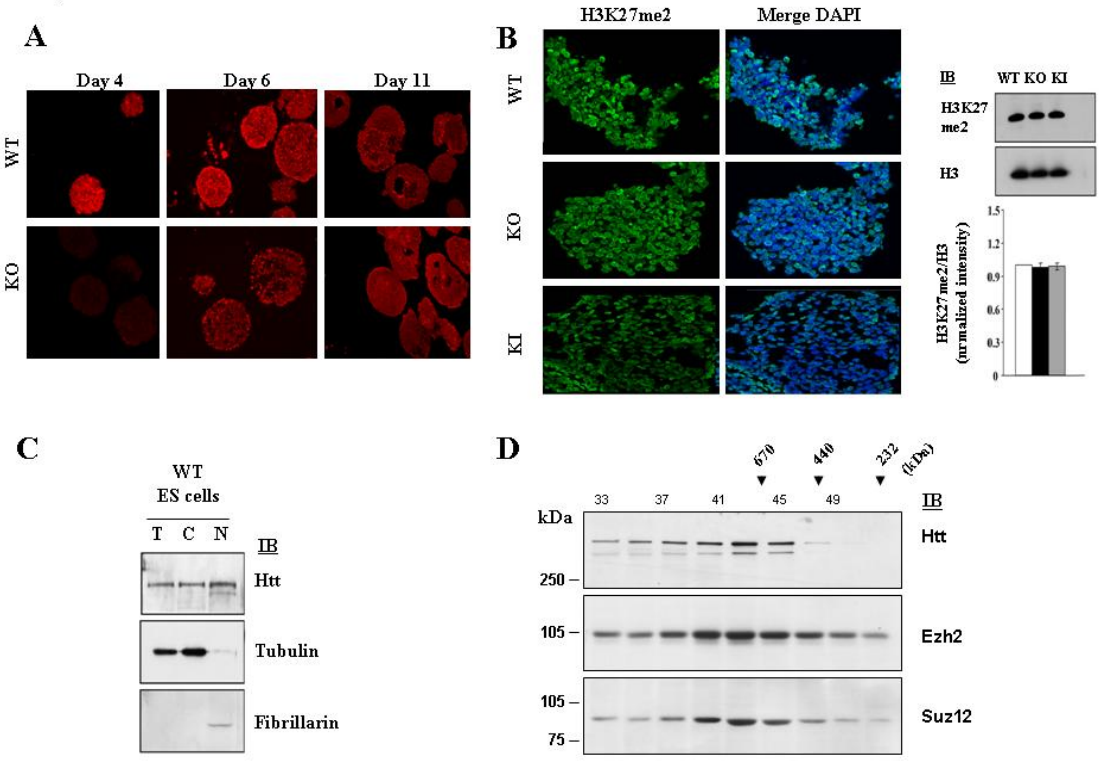
A
Day 4
Day 6
Day 11
WT
KO
B
H3K27me2
Merge DAPI
WT
KO
KI
IB
WT KO KI
H3K27 me2
H3
H3K27 me2/H3 (normalized intensity)
1.5
1.2
0.9
0.6
0.3
0
C
WT ES cells
T C N
IB
Htt
Tubulin
Fibrillarin
D
670
440
232
(kDa)
33
37
41
45
49
kDa
IB
250 –
Htt
105 –
Ezh2
105 –
75 –
Suz12

S Figure 4

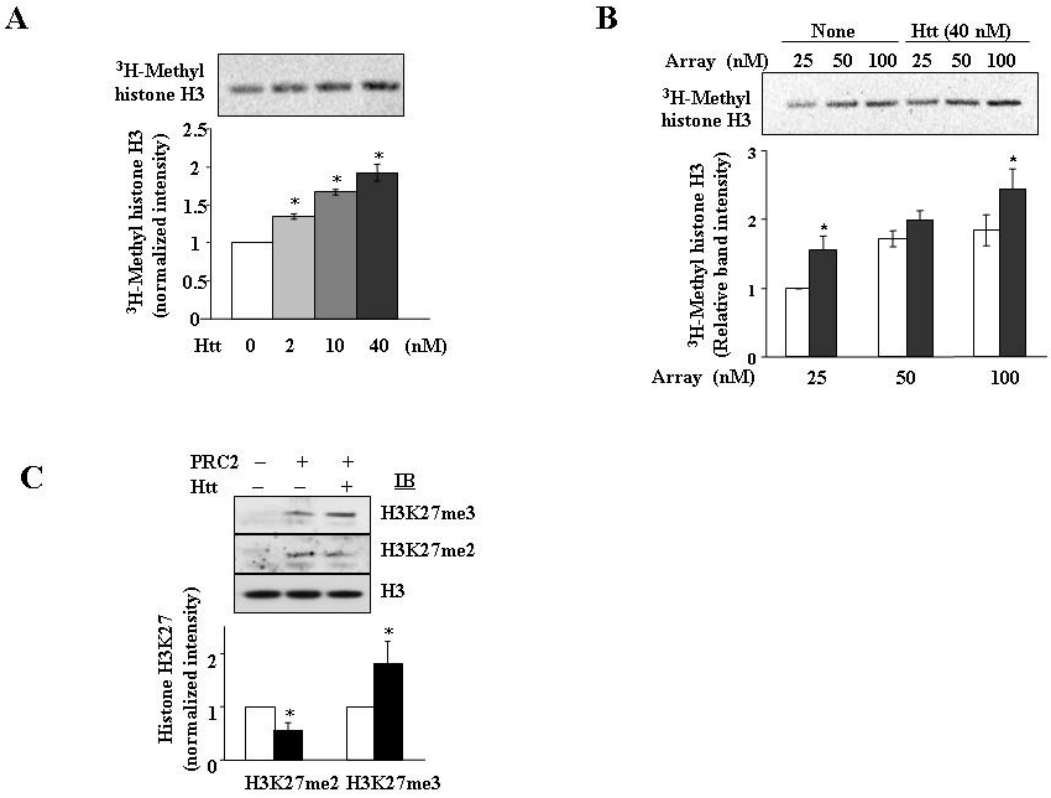
A
^{3}H-Methyl histone H3
^{3}H-Methyl histone H3 (normalized intensity)
2.5
2
1.5
1
0.5
0
Htt 0 2 10 40 (nM)
B
None
Htt (40 nM)
Array (nM) 25 50 100 25 50 100
^{3}H-Methyl histone H3
^{3}H-Methyl histone H3 (Relative band intensity)
3
2
1
0
Array (nM) 25 50 100
C
PRC2 – + +
Htt – – +
IB
H3K27me3
H3K27me2
H3
Histone H3K27 (normalized intensity)
2
1
0
H3K27me2 H3K27me3